PAPER

Dimensional characterization of extracellular vesicles using atomic force microscopy

IOP Publishing Measurement Science and Technology
Meas. Sci. Technol. **28** (2017) 034006 (8pp) doi:10.1088/1361-6501/28/3/034006

Dimensional characterization of extracellular vesicles using atomic force microscopy

N Sebaihi[1], B De Boeck[1], Y Yuana[2], R Nieuwland[2] and J Pétry[1]

[1] SMD, Belgian National Metrology Institute, Boulevard du Roi Albert II 16, 1000 Brussels, Belgium
[2] AMC, Academic Medical Centre, Meibergdreef 9, 1105 AZ Amsterdam, The Netherlands

E-mail: Noham.Sebaihi@economie.fgov.be

Received 15 June 2016, revised 7 October 2016
Accepted for publication 18 October 2016
Published 23 January 2017

Abstract

Extracellular vesicles (EV) are small biological entities released from cells into body fluids. EV are recognized as mediators in intercellular communication and influence important physiological processes. It has been shown that the concentration and composition of EV in body fluids may differ from healthy subjects to patients suffering from particular disease. So, EV have gained a strong scientific and clinical interest as potential biomarkers for diagnosis and prognosis of disease. Due to their small size, accurate detection and characterization of EV remain challenging. The aim of the presented work is to propose a characterization method of erythrocyte-derived EV using atomic force microscopy (AFM). The vesicles are immobilized on anti-CD235a-modified mica and analyzed by AFM under buffer liquid and dry conditions. EV detected under both conditions show very similar sizes namely ~30 nm high and ~90 nm wide. The size of these vesicles remains stable over drying time as long as 7 d at room temperature. Since the detected vesicles are not spherical, EV are characterized by their height and diameter, and not only by the height as is usually done for spherical nanoparticles. In order to obtain an accurate measurement of EV diameters, the geometry of the AFM tip was evaluated to account for the lateral broadening artifact inherent to AFM measurements. To do so, spherical polystyrene (PS) nanobeads and EV were concomitantly deposited on the same mica substrate and simultaneously measured by AFM under dry conditions. By applying this procedure, direct calibration of the AFM tip could be performed together with EV characterization under identical experimental conditions minimizing external sources of uncertainty on the shape and size of the tip, thus allowing standardization of EV measurement.

Keywords: biomaterials, extracellular vesicles, dimensional characterization, atomic force microscopy, tip convolution effect

(Some figures may appear in colour only in the online journal)

1. Introduction

Extracellular vesicles (EV) are sub-micrometer entities enclosed by a phospholipid bilayer and released from cells into their environment (figure 1) [1]. EV are nearly generated by every cell-type and are abundantly present in most biological fluids [2]. The EV composition is reflective of the parent cells, and consists of lipids, DNA, RNA and proteins, and EV expose specific receptors [3, 4]. Although considered as inert cellular debris initially, EV are now recognized as important mediators in intercellular communication and participate to many important biological processes [5, 6]. It has been shown that the concentration, composition and cellular origin of EV in body fluids differ between healthy subjects and patients suffering from diseases like myocardial infarction or cancer [7–9]. Therefore, there is a growing scientific and medical interest in cell-derived EV as valuable and non-invasive biomarkers.

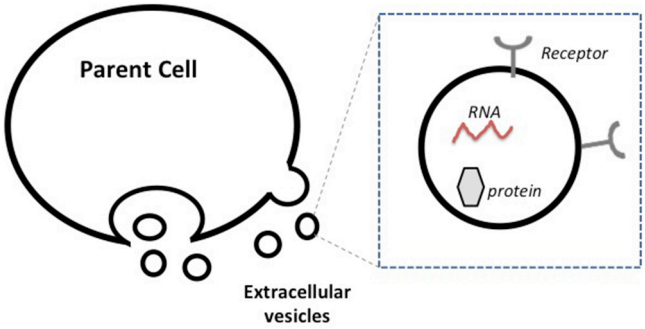

Figure 1. Schematic diagram of the structure of EV. Parent cell releases EV into the extracellular environment through different pathways. EV are intercellular communicators that may harbor various bioactive materials such as RNA, DNA or proteins. The EV membrane is a lipid bilayer containing receptors.

Making a medical decision requires reliable information obtained from routine analyses of body fluids composition. Human plasma that contains EV from platelets and erythrocytes is one of the most studied body fluids [10]. The comparison of measurement results between laboratories is of key importance in EV research. Nonetheless, the detection, classification, and quantitative analysis of EV remain challenging since these vesicles are highly heterogeneous in composition and size with diameters smaller than 100 nm and display low refractive index values [11]. Among the techniques available to study EV, flow cytometry is currently the most widely used in laboratories. However, the detection limit of this optical method is approximately 300 nm and allows to detect as discrete particles only a small fraction (1–2%) of the vesicles present in biological fluid samples [12, 13]. Moreover, the standardization of the technique remains difficult as the relationship between EV size and the measured light scattering is difficult to calibrate.

Atomic force microscopy (AFM) has been proposed as a more accurate technique to characterize EV [14, 15]. AFM is a versatile scanning probe technique widely used to image and study nano-objects and nanomaterials with a resolution down to the nanoscale. The ability of imaging soft samples without damaging in different environmental media (air and liquid) makes AFM a powerful tool for the study of biological samples including EV under physiological conditions (i.e. in buffer solution) [16, 17]. Moreover, from a metrological point of view, AFM is a measuring technique providing dimensional measurements that might be directly traceable to the SI [18, 19]. AFM allows measuring the out of plane dimension of nano-objects with sub-nanometer accuracy. The in-plane lateral resolution, however, is affected by the tip convolution effect, which occurs especially when features of similar or smaller radii than the AFM tip probe are measured. An AFM image results from the convolution of the shape of the probe and the shape of the sample, thus making protruding features to appear wider than in reality. Therefore, the characterization of the tip geometry and size is required to correct for this image artifact in order to obtain more accurate in-plane measurements. The dimensional characteristics of the tip can be extracted from external analyses of the probe (e.g. by electron microscopy), or by reconstruction from extra imaging of well-defined nanostructures with the same probe [20]. The main drawback of these methods is that those characteristics are assessed from external analyses, thus under different experimental conditions like for instance temperature, state of the AFM tip, force between probe and sample or varying scan speed. An approach consisting in the codeposition of the sample to analyze with particles of well-known dimension enable however an *in situ* calibration of the measurement [21–23].

Several studies have characterized EV from different human body fluids by AFM, including blood [14, 15, 24–26], saliva [27] and synovial fluid [28, 29]. These investigations were mainly devoted to the isolation, detection, qualitative analysis of the morphology and size of different types of cell-derived EV, to the membrane composition, and mechanical properties. The present work is dedicated to the morphological and dimensional characterization of EV using AFM, and is particularly focused on the accurate size determination necessary for the standardization of EV measurement. Erythrocyte-derived EV from human body fluids were immobilized on a selective antibody-modified mica substrate and characterized by tapping-mode AFM. The morphology and size of the EV were compared under liquid and dry conditions. Afterwards, an *in situ* calibration of the tip was performed through the codeposition of spherical reference polystyrene (PS) nanobeads and EV by capture on a poly-L-lysine-modified mica substrate. For spherical nanobeads, the height measured by AFM is equal to the real diameter of the particles. Therefore, comparing the measured diameter to the height of these spherical PS nanobeads allows to evaluate the magnitude of the tip broadening and to determine the tip size characteristics. Based on this information, the measured diameter of the EV is corrected for the tip convolution artifact through a simple geometrical model.

2. Materials and methods

2.1. EV sample preparation and immobilization on antibody-modified mica surface

Samples containing erythrocyte-derived extracellular vesicles were prepared as previously described [30]. To capture EV, the surface of mica substrate was modified following a protocol based on the selective recognition between EV and a complementary immobilized antibody.

The surface of the mica disks was modified as follows. The surface of the mica disks was functionalized with amine groups using a solution containing 55% (w/v) ethanolamine (Sigma Aldrich, Munich, Germany) in dimethylsulfoxide (DMSO) (99.7% purity, Sigma Aldrich). Molecular sieve beads (0.3 nm, Sigma Aldrich) were added to absorb the water formed later during the amine reaction on the mica surface. This solution was heated at 70 °C until the ethanolamine was completely dissolved. Next, freshly cleaved mica sheets (Ted Pella, Redding, CA), with a diameter of 10 mm, were incubated overnight in the ethanolamine solution. Subsequently, the amine-functionalized mica sheets were rinsed twice in DMSO (70 °C) and twice in absolute ethanol (Sigma Aldrich)

at room temperature. These mica sheets were dried under a N_2 flow. Prior to antibody coupling, the modified mica were incubated for 3 h with 1 mg ml^{-1} ethylene glycol-bis(2-aminoethyl ether)-N, N, N′, N′-tetraacetic acid (EGTA, Sigma Aldrich) in chloroform (Fisher Scientific) containing 0.5% (v/v) triethylamine (Fisher Scientific) to activate the amine functions. The mica sheets were then washed in chloroform, dried under N_2, and glued on a steel disk. Fifity μl of mouse anti-human CD235a antibody clone JC159 (Dako, Heverlee, Belgium) (0.01 mg ml^{-1}) was applied to the modified mica and incubated for 30 min at room temperature. The anti-CD235a was covalently attached to the mica while the excess of antibody was removed by washing with phosphate buffer saline solution PBS (Fisher Scientific, pH 7.4). Before the deposition of the EV, the topography of the modified-mica was evaluated (data not shown) to ensure that the samples with a fully covering antibodies layer were retain for the analysis. The mica surface was entirely covered by antibodies, leaving a clean substrate that exhibits a root mean square roughness of 1.1 nm over a 10×10 μm^2 sample area. A fraction of erythrocyte-derived EV stored at −80 °C was then thawed on melting ice. An EV fraction (20 μl) was applied to the anti-CD235a-coated mica surface and incubated for 30 min at room temperature to allow the binding of the EV to the anti-CD235a. The mica was eventually washed twice with PBS buffer to remove unbound EV.

2.2. Sample preparation for AFM-tip convolution evaluation

A freshly cleaved mica disk was treated with 20 μl of poly-L-lysine (Ted Pella, Redding, CA) during 15 min at room temperature. The modified mica was then washed with ultrapure water and dried under a N_2 flow. An aqueous colloidal suspension of polystyrene nanobeads presenting a unimodal size distribution (AFM measurement, mode~94 nm) extending from ~104 to ~6 nm with a negative skew was purchased from Kisker Biotech GmbH & Co. and diluted to a concentration of 10^{-2} mg ml^{-1}. A 20 μl fraction of the nanobeads suspension was applied to the modified mica during 15 min allowing the poly-L-lysine to electrostatically capture the nanoparticles. The substrate was then washed with water and dried under N_2. Afterwards, a 20 μl erythrocyte-derived EV fraction was applied to the mica during 1 h, gently rinsed with ultrapure water and let dry for at least 1 h at room temperature.

2.3. AFM analysis

AFM measurements were performed using a Dimension 3100 AFM equipped with a Nanoscope V controller (Veeco) operating in tapping-mode. Standard silicon nitride cantilevers (OMCL-240TS, Olympus, Japan), with resonant frequencies ranging between 66 and 89 kHz, and spring constants ranging between 1.4 and 3.5 Nm^{-1}, were used. Imaging was performed at a rate of 0.5 Hz and under soft-tapping conditions, i.e. keeping the ratio between the set-point amplitude and the free amplitude (between 30 and 50 nm) of the cantilever above 70%. All measurements were performed in temperature (23 °C ± 1 °C) and humidity (45% ± 5%) controlled laboratories. For experiments under dry conditions, samples were gently rinsed with ultrapure water and let dry at room temperature. For measurements in liquid, a Veeco glass fluid cell was mounted on the AFM piezoelectric scanner and an 80 μl PBS droplet was used as imaging medium. The AFM instrument was calibrated in the three directions using a NIST traceable VLSI step height standard (pitch size 3.00 ± 0.02 μm and step height of 15.7 ± 2.9 nm) in order to ensure the traceability of the measurements to the SI. 10×10 μm^2 and 20×20 μm^2 AFM images were recorded at 1024×1024 and 4096×4096 pixels, respectively. All the images were analyzed using SPIP software (Image Metrology A/S, www.imagemet.com). A second order flattening was applied to AFM images and the particle analysis function (Particle and Pore analysis) of SPIP software was used to detect and measure the size of the particles.

3. Results and discussion

3.1. Morphological and dimensional characterization of EV

Erythrocyte-derived EV are usually identified by the binding of antibodies to a protein uniquely expressed on erythrocyte membrane, namely glycophorine A (CD235a) [31]. Therefore, the immobilization protocol presented here involves the capture of erythrocyte-derived EV using anti-CD235a antibody chemically attached to a mica substrate. The AFM images of the representative topography of erythrocyte-derived EV immobilized on anti-CD235a-modified mica are presented in figure 2. AFM imaging was performed under near physiological liquid conditions (figure 2(a)) and after drying the sample at room temperature during 1 h (figure 2(b)). All experiments were performed at a scan speed of 0.5 Hz under soft tapping-mode conditions. The imaging force was controlled and minimized keeping the ratio between the amplitude set-point and the free oscillation amplitude (30–50 nm) of the cantilever as high as possible. It has been found that keeping this ratio above 70% ensures a good tracking of the EV without damaging. The immobilization protocol allows to successfully detect EV on both images appearing as discrete circular light grey particles of various sizes. The enlarged 3D views of two particles pointed out on the respective 2D images show that the EV exhibit the same protruding rounded shape morphology in both media. Very small particles and extra material remaining from sample preparation like membrane debris are also observed on the background surrounding the vesicles.

To characterize the dimension of the vesicles, two parameters are defined and measured: (1) the height, i.e. the out of plane dimension and (2) the watershed diameter (in-plane), i.e. the diameter of a disk having the same surface as the area enclosed by the contour of the particle detected by the watershed method in the SPIP software used to analyze the AFM images. This detection method is a classical image segmentation approach that allows to detect the closed contour of the particles from the background [32].

Histograms of the measured heights and watershed diameters of the EV are presented in figures 3(a) and (b), respectively. Data were collected from the analysis of several tens of AFM images. Only discrete vesicles showing well-defined

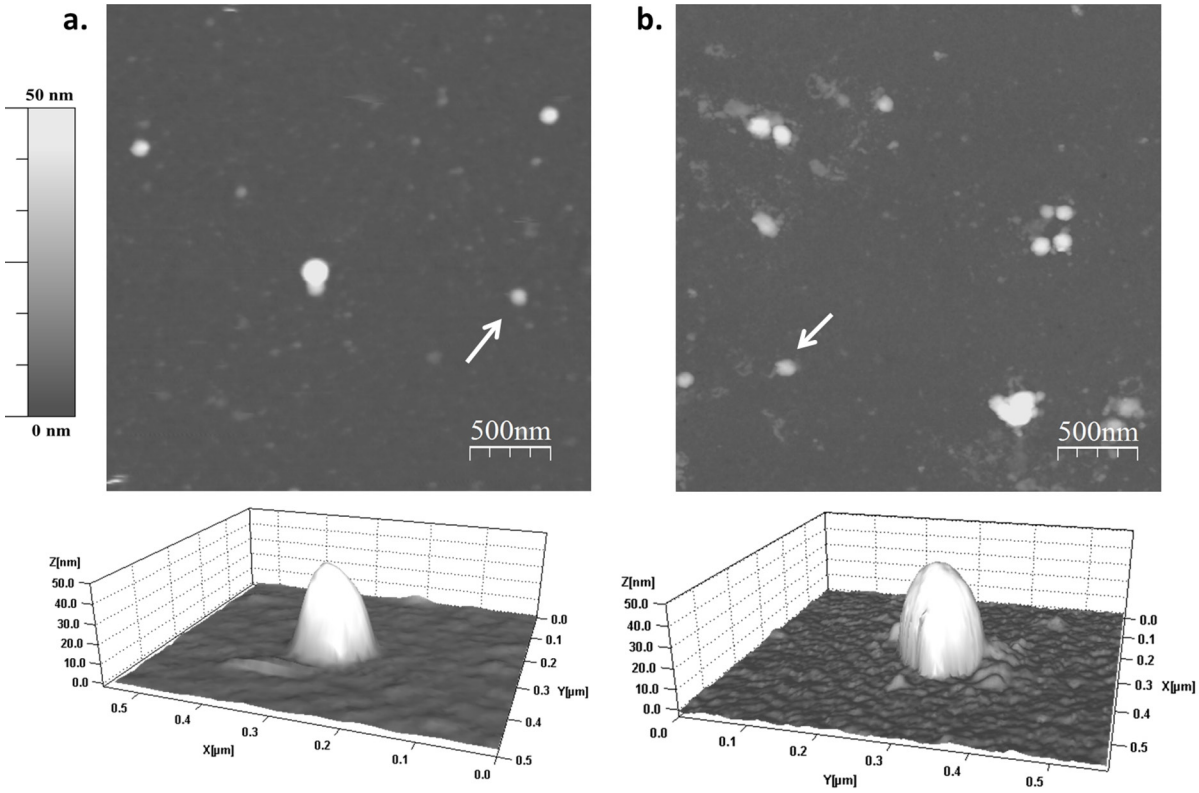

Figure 2. 3×3 μm² tapping-mode AFM images of the topography of erythrocyte-derived EV immobilized on antibody-modified mica. Imaging was performed in PBS solution (a) and under dry conditions (b) at room temperature. EV appear as circular light grey particles on both images. Enlarged 3D views of the EV indicated by white arrows are presented below respective images. The z scale of the 3D views have been magnified to improve visualization.

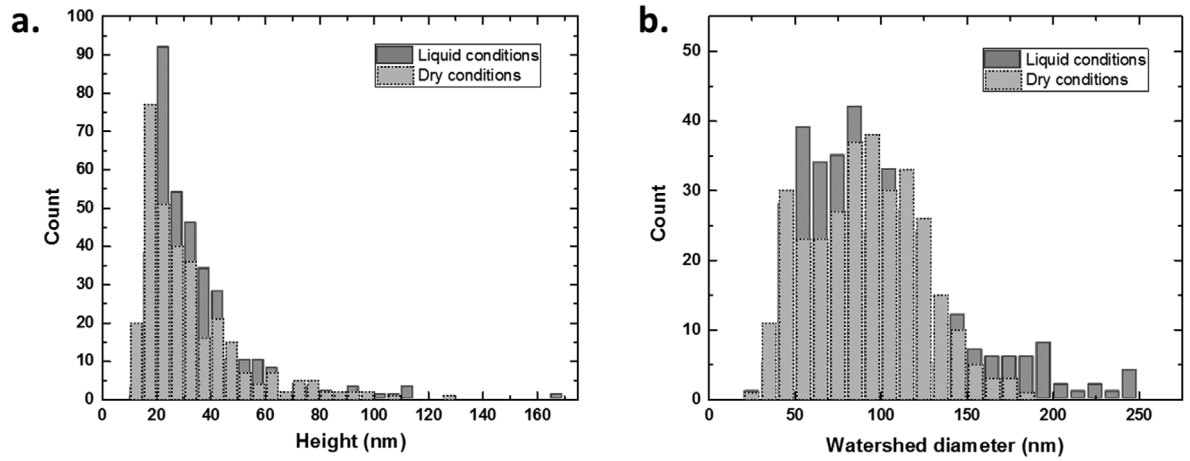

Figure 3. Size distributions of the height (a) and the watershed diameter (b) of EV measured under liquid and dry conditions. The data were obtained from the analysis of around twenty 10×10 μm² AFM images.

boundaries without agglomerate were considered for the statistics. The statistic data are presented as mean ± standard deviation (mode). Based on the analysis of 352 detected particles, EV measured in liquid medium present a mean height of 34.0 ± 18.8 nm (27.1 nm) and a mean watershed diameter of 97.7 ± 44.0 nm (82.5 nm). Based on 316 detected particles, EV measured under dry conditions present a mean height of 31.7 ± 18.7 nm (23.9 nm) and a mean watershed diameter of 91.6 ± 32.6 nm (90.3 nm). In both cases height distributions extend from ~5 nm to ~180 nm while watershed diameter distributions extend from ~10 nm to ~250 nm. At this point, it is important to note that measurements performed under liquid and dry media show similar morphologies and sizes. The vesicles exhibit an in-plane diameter that is 3 times greater than the height. The size-range of the EV is consistent with values previously reported in AFM studies of other cellular origin derived EV [14, 15, 26–29].

To evaluate the extend of this trend, the stability of EV morphology over time was assessed. Figure 4 presents the evolution of the height and watershed diameter of EV with

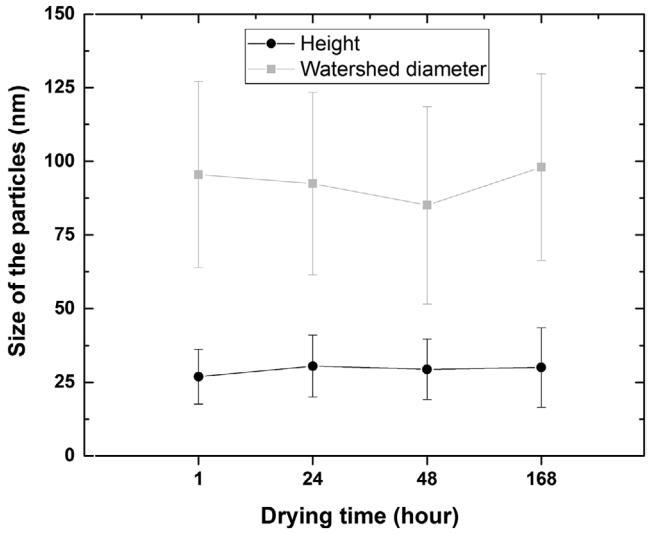

Figure 4. Evolution of the size (mean values) of the EV with the drying time of the sample at room temperature. Error bars represent the standard deviation calculated from 70 to 100 detected particles.

respect to the drying time. The sample was dried under ambient conditions for a period of time extending from 1 h to 168 h. Each point of the graph was calculated from the analysis of 5 different AFM images (~100 discrete particles) of fresh areas of the same sample with the same AFM probe. No significative variation of the height and the watershed diameter of the EV is observed. This indicates that the morphology and size of the erythrocyte-derived EV are surprisingly stable over drying time as long as 7 d. Hardij *et al* have compared the morphology and size of breast cancer cell-derived EV under physiological and dry conditions by AFM [15]. They observed that EV measurements in air were 6–10 times smaller than in liquid. That observation was ascribed to the shrinkage of the EV due to the evaporation of the liquid inside the vesicle during the drying procedure. The behavior of the vesicles presented here contrasts with these previous observations which may be due to EV derived from different cell origin. Further investigation should employ the same procedure using EV from different cell origin of healthy subjects to assess the composition of the EV after drying procedure.

3.2. Evaluation of the tip convolution artifact

The in-plane dimension of the EV is shown to be approximately 3-fold larger than the out of plane dimension. The shape of the vesicles will then be approximated by an oblate spheroid (ellipsoid) geometry described by the in-plane diameter ($a = b$) and the height (c) parameters. This shape morphology is obviously partly attributed to the lateral broadening artifact arising from the tip convolution effect inherent to AFM measurements. However, other effects such as the interaction of the vesicle with the antibody-modified mica surface and the deformation arising from the imaging force exerted by the tip also play a role. The magnitude of this tip hindrance effect is described by geometrical considerations and has relatively the greatest broadening on features of similar or smaller radii than the AFM tip, which is the case for the studied EV samples. The broadening artifact has to be determined to precisely measure the diameter of the vesicles. This is done by measuring synthetic reference nanoparticles. Considering spherical nanoparticles, the height measured by AFM corresponds to the real diameter of the particles [33]. The diameter obtained by the watershed detection method greatly depends on the parameters chosen for the detection and the corresponding contours have no fixed level relative to the background. Therefore the tip broadening artifact could not be unambiguously determined. On the contrary, the mid-height diameter, defined as the diameter of a disk having the same surface as the area enclosed by the contour of the particle at half height, is determined and used for the tip calibration.

To model the broadening effect of the particle, the shape of the tip is approximated by a right circular cone with a partial sphere at the bottom [34]. In this model, the tip is also assumed to interact perpendicularly to the sample surface with no tilt. The tip shape is characterized by the half opening angle of the cone α and the radius of the sphere (figure 5). The tip shape parameters can be calculated by comparing the height (z) of the spherical nanoparticles and the measured mid-height diameter (d_{m}). Indeed, it can be derived analytically that, if the height is large enough, there is a linear relationship between the mid-height diameter and the height (equation (1)), where the slope and the intercept are denoted as a and b, respectively (equation (2)). These expressions can be solved to α and r (equations (3) and (4)). Estimation of a and b, by performing a linear regression on the measured mid-height diameters and heights, then allows to determine the free parameters α and r in this tip shape surface model.

$$d_{\mathrm{m}} = \frac{1}{\cos\alpha} z + 2\,r\,\frac{(1-\sin\alpha)}{\cos\alpha} \tag{1}$$

$$a := \frac{1}{\cos\alpha} \text{ and } b := 2r\,\frac{(1-\sin\alpha)}{\cos\alpha} \tag{2}$$

$$\alpha = \cos^{-1}(a^{-1}) \tag{3}$$

$$r = \frac{b\cos\alpha}{2(1-\sin\alpha)} \tag{4}$$

3.3. EV characterization after tip shape deconvolution

For the purpose of characterizing the tip shape, spherical polystyrene nanobeads were used. The nanoparticles present a unimodal height distribution (mode ~94 nm) extending from ~6 to ~104 nm with a negative skew. The height of these nanobeads extends over the same range as the EV, making them good candidates for correcting the tip broadening effect. Instead of reconstructing the tip convolution from an extra imaging, the PS nanobeads are concomitantly deposited with EV on poly-L-lysine-modified mica and analyzed by AFM under dry conditions. This procedure ensures to keep experimental conditions identical during the calibration of the tip. It should be noted that in liquid the EV and PS nanobeads do not stick tightly enough to the poly-L-lysine layer to be measured by AFM. Figure 6 presents the correlation between the height and the

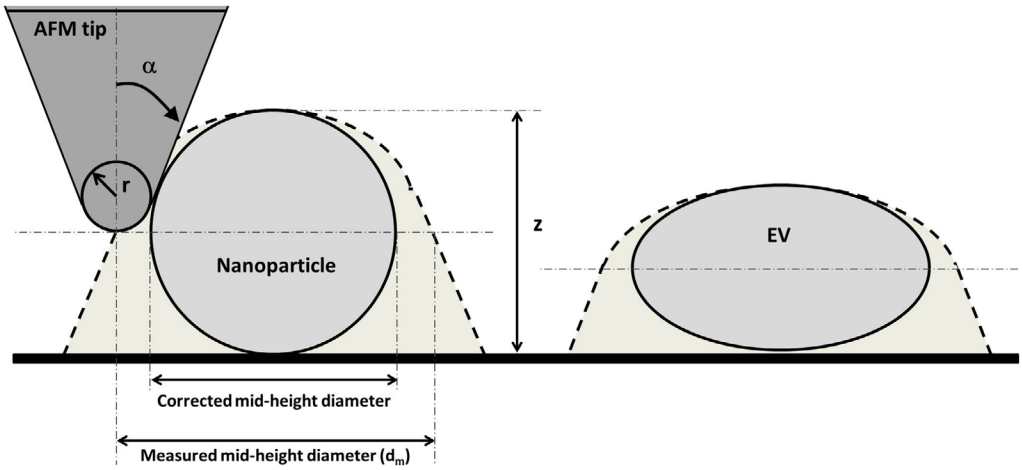

Figure 5. Schematic representation of the tip convolution effect on a spherical nanoparticle and an ellipsoidal EV. The AFM tip is modeled by a right circular cone with a half opening angle α and a sphere of radius r at the apex. Diameters of the particles are determined at mid-height.

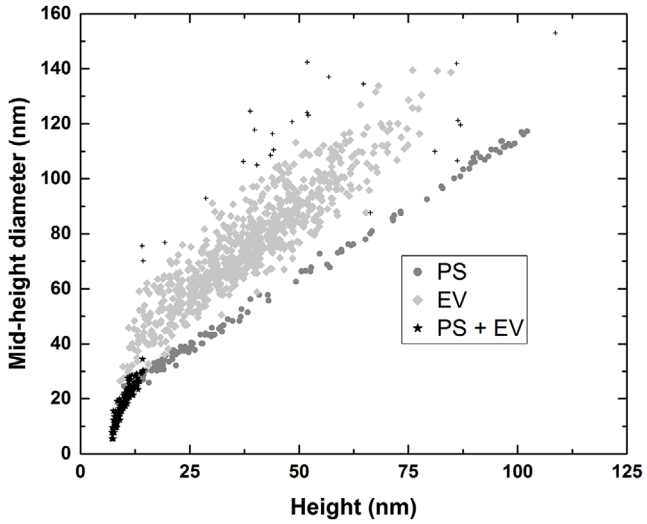

Figure 6. Correlation diagram between the mid-height diameter and the height of PS nanobeads and EV codeposited on poly-L-lysine modified mica. The data are extracted from a unique 20 × 20 μm² AFM image (1163 detected particles). Data represented on the graph by (+) are rejected from the analysis.

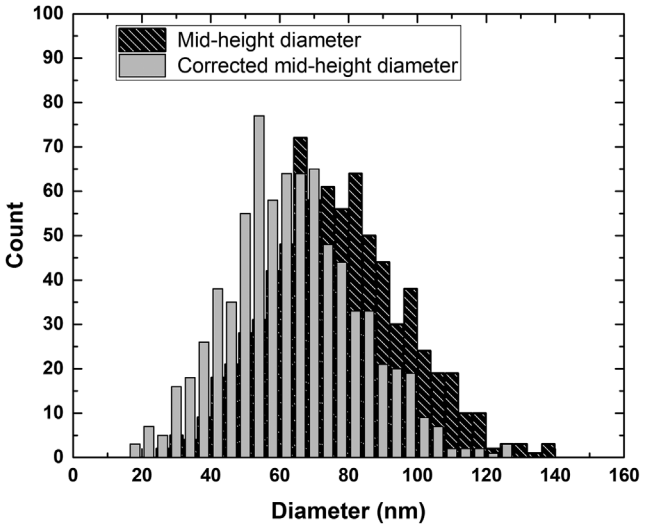

Figure 7. Correction of the mid-height diameter of the particles (775 particles).

mid-height diameter of PS nanobeads and EV obtained from a unique 20 × 20 μm² image (1163 detected particles). Data were analyzed using a statistical robust trimmed model based on data clustering [35]. In this clustering method, a bivariate normal distribution is assumed for each group of data in order to identify which data belongs to the same group or cluster. According to this method, three data groups can be extracted and are highlighted in figure 6. Two main distinct clusters of particles are clearly distinguishable. The first group (dark grey circles), showing high aspect ratios (height/mid-height diameter) and a linear relationship between the mid-height diameter and the height, clearly corresponds to the well-defined PS nanoparticles. The second group (light grey diamonds) consists of more dispersed data with a lower aspect ratio. That is consistent with the spheroidal shape morphology of the EV. The difference in morphologies allows clearly distinguishing the two sets of particles. For smaller size particles (black stars, height < 15 nm), data cannot be discriminated on the basis of their aspect ratio anymore as approaching the lateral resolution of the instrument, which is mainly limited by the pixel size and the dimension of the tip apex. The dispersion of the second group of data is inherent to the biological nature of the vesicles but also includes all the deformation contributions arising from the measurement like the EV-substrate interaction and the imaging force exerted by the probe. The effect of the imaging force could be studied by looking at the evolution of the EV morphology and size while varying the force applied by the AFM tip to the sample, as previously presented in several studies on biomaterials [27, 36].

A total least squares regression via principal components analysis on the PS nanoparticles data cluster provides a regression line of $d_m = 1.034z + 12.108$ nm. These slope and intercept values determine a cone half angle $\alpha = 14.7°$ and a sphere radius $r = 7.8$ nm. These values are consistent with the specifications reported by the manufacturer based on electronic microscopy characterization. The half angle and radius

parameter values fix the tip shape and enable to determine the broadening effect for each EV by using a mathematical derivation relying on a rotation symmetric oblate spheroid shape assumption for the EV. The correction for the tip broadening is then applied to the mid-height diameter of the EV. Figure 7 presents the diameter distributions of the EV before and after the correction for the tip convolution effect. An average correction of 12.1 nm is observed going from a mean mid-height diameter of 76.2 ± 19.9 nm for the EV to a mean value of 64.1 ± 19.0 nm after correction. This corrected diameter is associated with a mean height of 38.8 ± 14.5 nm. The mean calculated diameter of a sphere having the same volume as the ellipsoid is 54.0 ± 17.2 nm and reflects the free state of the EV in solution. The size values reported here are far below the detection limit of conventional measuring instruments used in clinical laboratories such as flow cytometry. Moreover, the detection limit of these instruments strongly depends on the size range of the EV, each instrument presenting a different minimum detectable size for the same sample [37]. Therefore, the knowledge of the real size of the EV is particularly relevant to clinical research. That makes AFM a potential measurement instrument for the characterization of EV. The protocol presented in this work contributes to the standardization of EV measurements and might be applied to other dimensional characterizations of various biomaterials and non-spherical nanoparticles using AFM. The determination of an uncertainty budget accounting for the different sources of uncertainty involved in the measurement of biological samples by AFM would ensure the traceability of the measurement and as such further contribute to the development of the standardization of EV measurements. Besides the general sources of uncertainty involved in AFM measurements like height calibration procedure, non-linearity of the measuring sensor, thermal drift, noise level, scan speed or roughness of the background, the contributions of the geometrical models chosen for the tip and the EV, and the imaging force deformation of the EV should be investigated [18, 38, 39].

4. Conclusions

In this work, erythrocyte-derived EV immobilized on antibody-modified mica substrate have been characterized by tapping-mode AFM. This protocol allows successful detection and can be used to study the morphology and size of the particles under near physiological (in liquid) and dry conditions. EV appear homogenous in morphology presenting a spheroidal shape of similar size in both media. Surprisingly, EV size and shape are stable over drying time as long as 7 d. In order to improve the accuracy of the EV diameter measurements, a method to correct for the tip convolution effect is presented. EV are codeposited with reference nanoparticles on poly-L-lysine-modified mica and measured by AFM under dry conditions. The advantage of this method is to provide a measurement correction from a unique AFM analysis, under similar experimental conditions. The detected particles are discriminated on the basis of their aspect ratio. The size and shape of the AFM tip are then derived from the reference nanoparticles data considering a simple geometrical model to describe the probe. The calculated geometric parameters of the tip are consistent with manufacturer's parameters and used to correct back the diameter of the EV. The tip convolution effect is seen to have a magnification effect of about 19% on the lateral measurement.

The proposed method can be used to measure other biomaterials and non-spherical nanoparticles. Future work on the determination of an uncertainty budget regarding the measurement of biological samples by AFM would further contribute to the standardization of EV measurements.

Acknowledgments

The work in this project is part of the European Metrology Research Programme (EMRP) project 'Metrological characterization of microvesicles from body fluids as non-invasive diagnostic biomarkers' (www.metves.eu). The EMRP is jointly funded by the EMRP participating countries within the European Association of National Metrology Institutes (EURAMET) and the European Union.

References

[1] Diamant M, Tushuizen M E, Sturk A and Nieuwland R 2004 Cellular microparticles: new players in the field of vascular disease? *Eur. J. Clin. Invest.* **34** 392–401
[2] EL Andaloussi S, Mäger I, Breakefield X O and Wood M J a 2013 Extracellular vesicles: biology and emerging therapeutic opportunities *Nat. Rev. Drug Discov.* **12** 347–57
[3] Cocucci E and Meldolesi J 2015 Ectosomes and exosomes: Shedding the confusion between extracellular vesicles *Trends Cell Biol.* **25** 364–72
[4] Bang C and Thum T 2012 Exosomes: new players in cell–cell communication *Int. J. Biochem. Cell Biol.* **44** 2060–4
[5] van der Pol E, Böing A N, Harrison P, Sturk A and Nieuwland R 2012 Classification, functions, and clinical relevance of extracellular vesicles *Pharmacol. Rev.* **64** 676–705
[6] Yuana Y, Sturk A and Nieuwland R 2013 Extracellular vesicles in physiological and pathological conditions *Blood Rev.* **27** 31–9
[7] Anderson H C, Mulhall D and Garimella R 2010 Role of extracellular membrane vesicles in the pathogenesis of various diseases, including cancer, renal diseases, atherosclerosis, and arthritis *Lab. Invest.* **90** 1549–57
[8] Tesselaar M E T, Romijn F P H T M, Van Der Linden I K, Prins F A, Bertina R M and Osanto S 2007 Microparticle-associated tissue factor activity: a link between cancer and thrombosis? *J. Thromb. Haemost.* **5** 520–7
[9] Martins V R, Dias M S and Hainaut P 2013 Tumor-cell-derived microvesicles as carriers of molecular information in cancer *Curr. Opin. Oncol.* **25** 66–75
[10] Witwer K W *et al* 2013 Standardization of sample collection, isolation and analysis methods in extracellular vesicle research *J. Extracell. Vesicles* **2** 20360
[11] van der Pol E, Hoekstra A G, Sturk A, Otto C, van Leeuwen T G and Nieuwland R 2010 Optical and non-optical methods for detection and characterization of microparticles and exosomes *J. Thromb. Haemost.* **8** 2596–607
[12] Ayers L, Kohler M, Harrison P, Sargent I, Dragovic R, Schaap M, Nieuwland R, Brooks S A and Ferry B 2011 Measurement of circulating cell-derived microparticles by flow cytometry: sources of variability within the assay *Thromb. Res.* **127** 370–7

[13] van der Pol E, Van Gemert M J C, Sturk A, Nieuwland R and Van Leeuwen T G 2012 Single versus swarm detection of microparticles and exosomes by flow cytometry *J. Thromb. Haemost.* **10** 919–30
[14] Yuana Y, Oosterkamp T H, Bahatyrova S, Ashcroft B, Garcia Rodriguez P, Bertina R M and Osanto S 2010 Atomic force microscopy: a novel approach to the detection of nanosized blood microparticles *J. Thromb. Haemost.* **8** 315–23
[15] Hardij J, Cecchet F, Berquand A, Gheldof D, Chatelain C, Mullier F, Chatelain B and Dogné J-M 2013 Characterisation of tissue factor-bearing extracellular vesicles with AFM: comparison of air-tapping-mode AFM and liquid peak force AFM *J. Extracell. Vesicles* **2** 1–9
[16] Liu S and Wang Y 2010 Application of AFM in microbiology: a review *Scanning* **32** 61–73
[17] Allison D P, Mortensen N P, Sullivan C J and Doktycz M J 2010 Atomic force microscopy of biological samples *Wiley Interdiscip. Rev. Nanomed. Nanobiotechnol.* **2** 618–34
[18] Yacoot A and Koenders L 2011 Recent developments in dimensional nanometrology using AFMs *Meas. Sci. Technol.* **22** 122001
[19] Danzebrink H-U, Koenders L, Wilkening G, Yacoot A and Kunzmann H 2006 Advances in scanning force microscopy for dimensional metrology *CIRP Ann.* **55** 841–78
[20] Winzer A T, Kraft C, Bhushan S, Stepanenko V and Tessmer I 2012 Correcting for AFM tip induced topography convolutions in protein-DNA samples *Ultramicroscopy* **121** 8–15
[21] Vesenka J, Manne S, Giberson R, Marsh T and Henderson E 1993 Colloidal gold particles as an incompressible atomic force microscope imaging standard for assessing the compressibility of biomolecules *Biophys. J.* **65** 992–7
[22] Vesenka J 1996 Atomic force microscopy reconstruction of G-wire DNA *J. Vac. Sci. Technol.* B **14** 1413
[23] Abdelhady H G, Allen S, Ebbens S J, Madden C, Patel N, Roberts C J and Zhang J 2005 Towards nanoscale metrology for biomolecular imaging by atomic force microscopy *Nanotechnology* **16** 966–73
[24] Siedlecki C A, Wang I W, Higashi J M, Kottke-Marchant K and Marchant R E 1999 Platelet-derived microparticles on synthetic surfaces observed by atomic force microscopy and fluorescence microscopy *Biomaterials* **20** 1521–9
[25] Salzer U, Hinterdorfer P, Hunger U, Borken C and Prohaska R 2002 Ca^{++}-dependent vesicle release from erythrocytes involves stomatin-specific lipid rafts, synexin (annexin VII), and sorcin *Blood* **99** 2569–77
[26] Ashcroft B A, de Sonneville J, Yuana Y, Osanto S, Bertina R, Kuil M E and Oosterkamp T H 2012 Determination of the size distribution of blood microparticles directly in plasma using atomic force microscopy and microfluidics *Biomed. Microdevices* **14** 641–9
[27] Sharma S, Rasool H I, Palanisamy V, Mathisen C, Schmidt M, Wong D T and Gimzewski J K 2010 Structural-mechanical characterization of nanoparticle exosomes in human saliva, using correlative AFM, FESEM, and force spectroscopy *ACS Nano* **4** 1921–6
[28] György B *et al* 2011 Detection and isolation of cell-derived microparticles are compromised by protein complexes resulting from shared biophysical parameters *Blood* **117** e39–48
[29] Junkar I, Šuštar V and Frank M 2009 Blood and synovial microparticles as revealed by atomic force and scanning electron microscope *Open Autoimmun. J.* **1** e50–8
[30] Yuana Y, Böing A N, Grootemaat A E, van der Pol E, Hau C M, Cizmar P, Buhr E, Sturk A and Nieuwland R 2015 Handling and storage of human body fluids for analysis of extracellular vesicles *J. Extracell. Vesicles* **4** 29260
[31] Shet A S 2008 Characterizing blood microparticles: technical aspects and challenges *Vasc. Health Risk Manag.* **4** 769–74
[32] Klapetek P, Valtr M, Nečas D, Salyk O and Dzik P 2011 Atomic force microscopy analysis of nanoparticles in non-ideal conditions *Nanoscale Res. Lett.* **6** 514
[33] Nicolet A *et al* 2016 Inter-laboratory comparison on the size and stability of monodisperse and bimodal synthetic reference particles for standardization of extracellular vesicle measurements *Meas. Sci. Technol.* **27** 035701
[34] Seah M P, Spencer S J, Cumpson P J and Johnstone J E 2000 Sputter-induced cone and filament formation on InP and AFM tip shape determination *Surf. Interface Anal.* **29** 782–90
[35] Fritz H, García-Escudero L A and Mayo-Iscar A 2012 tclust : an R package for a trimming approach to cluster analysis *J. Stat. Softw.* **47** 1–26
[36] Jin A J, Prasad K, Smith P D, Lafer E M and Nossal R 2006 Measuring the elasticity of clathrin-coated vesicles via atomic force microscopy *Biophys. J.* **90** 3333–44
[37] van der Pol E, Coumans F A W, Grootemaat A E, Gardiner C, Sargent I L, Harrison P, Sturk A, van Leeuwen T G and Nieuwland R 2014 Particle size distribution of exosomes and microvesicles determined by transmission electron microscopy, flow cytometry, nanoparticle tracking analysis, and resistive pulse sensing *J. Thromb. Haemost.* **12** 1182–92
[38] Klapetek P, Nečas D, Campbellová A, Yacoot A and Koenders L 2011 Methods for determining and processing 3D errors and uncertainties for AFM data analysis *Meas. Sci. Technol.* **22** 025501
[39] Delvallée A, Feltin N, Ducourtieux S, Trabelsi M and Hochepied J F 2016 Toward an uncertainty budget for measuring nanoparticles by AFM *Metrologia* **53** 41–50